JOURNAL OF Materials CHEMISTRY

$FeCo–SiO_2$ nanocomposite aerogels by high temperature supercritical drying

Maria F. Casula, Anna Corrias* and Giorgio Paschina

Dipartimento di Scienze Chimiche, Università di Cagliari, Complesso Universitario di Monserrato, S.S. 554 bivio per Sestu, 09042 Monserrato, Cagliari, Italy. E-mail: corrias@unica.it; Fax: +39 070 6754388; Tel: +39 070 6754351

Received 6th November 2001, Accepted 26th February 2002
First published as an Advance Article on the web 28th March 2002

$FeCo–SiO_2$ nanocomposite aerogels were prepared by high temperature supercritical drying of alcogels obtained using tetraethoxysilane, iron nitrate and cobalt nitrate as precursors. The structural evolution of the samples at the various stages of the preparation was studied by thermal analysis, transmission electron microscopy, nitrogen physisorption measurements and X-ray diffraction. Different experimental conditions of the supercritical drying process give rise to different porous structures in the silica matrix which have a strong influence on the formation of the FeCo alloy nanoparticles. Bcc FeCo alloy nanoparticles of the expected composition are obtained in the microporous samples while in the mesoporous samples a bcc alloy with a lower Co content is obtained which is accompanied by pure fcc Co.

Introduction

The sol–gel method has proved to be a valuable method for producing nanocomposite materials constituted of metal nanoparticles embedded into an amorphous silica matrix which are of interest because of their peculiar physical and chemical properties.[1–3] In particular, final products with different characteristics can be obtained by varying the sol–gel process parameters, which is a key point when materials' properties need to be finely tuned. So far a great deal of work has been done on the preparation and characterization of single metal[1–7] and metal oxide nanoparticles[8–11] while not many papers have been devoted to alloy nanoparticles dispersed in amorphous silica.

Iron–cobalt alloys have attracted much attention because of their interesting magnetic properties.[12,13] Since the magnetic properties are strongly influenced by particle size[14] and they change dramatically in the nanometer range, it is very important to investigate the possibility of stabilizing the FeCo alloy at the nanometer scale. Recently, the sol–gel method was used to prepare $FeCo–SiO_2$ nanocomposites in the form of a xerogel.[15] The method was successful for the formation of FeCo alloy nanoparticles using metallic acetate precursors while metallic nitrate precursors gave rise to an fcc Co phase with the iron still present in an oxidized phase. However, nitrate precursors can offer some advantages with respect to acetates since they are highly soluble in ethanol and completely decompose at a relatively low temperature. This means that the sol–gel process can be carried out with a low H_2O : tetraethoxysilane (TEOS) ratio which is an important parameter in determining the characteristics of the alcogel.[16] Moreover, the low water content makes less arduous the preparation of aerogel nanocomposites by high temperature supercritical drying since the supercritical parameters for ethanol are much lower than those of water.

Aerogel materials are characterized by high surface area, high pore volume and low density, as a consequence of the drying process.[16,17] In fact, the original skeletal structure of the alcogel can be preserved when the solvent is removed above its critical parameters, T_c and P_c. In contrast xerogels, obtained by slow evaporation of the solvent, are relatively dense materials since the original porous structure of the wet gel collapses as a consequence of the capillary forces at the liquid–vapor interface within the pores.[16] Recently, high temperature supercritical drying was successfully applied to prepare $NiO–SiO_2$ and $Fe_2O_3–SiO_2$ nanocomposite aerogels with very high surface areas.[18,19] Moreover, by varying the supercritical drying conditions, the porous structure of both the nanocomposite aerogels and the aerogel silica matrix can be tailored.[18–20] These papers have shown that the drying conditions have an important role in the evolution of the precursors of the sol–gel process; in fact, nanocomposite xerogels and aerogels prepared starting from the same alcogels can be constituted of different nanophases.[18,19]

Therefore, the aim of this work is to test the possibility of applying the sol–gel method to the preparation of $FeCo–SiO_2$ nanocomposites in the form of aerogels, starting from iron nitrate and cobalt nitrate as precursors for the FeCo alloy nanoparticles, and tetraethoxysilane (TEOS) as the precursor for SiO_2. A comparison with the xerogel nanocomposites reported in ref. 15 will be discussed. The samples at the different stages of the sol–gel process were characterized by thermogravimetric analysis (TG), differential thermal analysis (DTA), N_2-physisorption, X-ray diffraction (XRD) and transmission electron microscopy (TEM).

Experimental

Iron–cobalt–silica aerogel nanocomposite materials were prepared by the sol–gel method; in all the samples the total metal content was kept equal to 10 wt% while the Fe : Co molar ratio was varied ($Fe_{70}Co_{30}$, $Fe_{50}Co_{50}$, $Fe_{30}Co_{70}$). Two samples containing either only Fe or Co (Fe_{100}, Co_{100}) were also prepared for comparison.

$Fe(NO_3)_3·9H_2O$ (Aldrich, 98%) and $Co(NO_3)_2·6H_2O$ (Aldrich, 98%) were dissolved in ethanol (Carlo Erba, 95%) and then added to a solution of TEOS (Aldrich, 98%) in ethanol (Carlo Erba, 95%). A few drops of concentrated HNO_3 (Carlo Erba, 70%) were added in order to achieve a pH value between 0.6–0.8. After vigorous stirring for 1 h, the sol was allowed to gel at room temperature in a Teflon beaker (initial surface to volume ratio 0.4); the gelation time was approximately 14 days for all samples.

The gels were submitted to high temperature supercritical drying in an autoclave (Parr, 300 cm^3) filled with an

appropriate amount of ethanol. Two different conditions of supercritical drying were used, which will be hereafter called A1 and A2, by varying the heating ramp, the solvent used to fill the autoclave and the initial pressure in the autoclave, P_i. Specifically, in the A1 procedure the autoclave is filled with 95% ethanol, purged with nitrogen and heated up to 250 °C at a rate of 5 °C min^{-1} and up to 300 °C at 1 °C min^{-1}. The A2 procedure uses absolute ethanol to fill the autoclave and an initial pressure of nitrogen in the autoclave of 7 atm; the autoclave is then heated up to 200 °C at 1 °C min^{-1} and up to 300 °C at 0.5 °C min^{-1}. Conditions A1 and A2 were selected on the basis of a study of nanocomposite aerogels and their silica matrix which indicated that a prevalent mesoporous and microporous structure can be obtained respectively.[18–20]

After supercritical drying, the aerogel samples were powdered and calcined at 350 °C in static air for 1 h in order to eliminate the organics and stabilize the intermediate products. After calcination the samples were submitted to a reduction treatment under H_2 flow at 800 °C for 2 h. The thermal treatment conditions were identical to those used for xerogel $FeCo–SiO_2$ nanocomposites.[15]

Thermal gravimetric analysis (TG) and simultaneous differential thermal analysis (DTA) were carried out on a Mettler-Toledo TGA/SDTA 851. Thermal analysis data were collected in the 25–1000 °C range, under oxygen flow (heating rate = 10 °C min^{-1}; flow rate = 50 ml min^{-1}).

TEM micrographs were recorded on a JEOL 200CX microscope operating at 200 kV. The samples were dispersed in *n*-octane and dropped onto a conventional carbon-coated copper grid.

Textural analysis was carried out on a Sorptomatic 1990 System (Fisons Instruments), by determining the nitrogen adsorption–desorption isotherms at 77 K. Before analysis, the samples were heated up to 200 °C at a rate of 1 °C min^{-1} under vacuum. The specific surface area (S_{TOTAL}) and the total pore volume (V_p) were assessed by the Brunauer–Emmett–Teller (BET) method.[21,22] The microporous volume (V_{MICRO}) and the surface area pertaining to the mesopores (S_t) were obtained from the t-plots.[23–24] The t-plots were calculated by the n-method of Lecloux,[25] where the choice of the standard isotherm is based on the C_{BET} value of the sample under testing (*i.e.* the extent of adsorbate–adsorbent interaction). For highly microporous samples, the specific surface area and the micropore volume were obtained using the Dubinin method.[21,26]

XRD spectra were recorded on a X3000 Seifert diffractometer equipped with a graphite monochromator on the diffracted beam. The scans were collected within the range of 10–120° (2θ) using Cu-Kα radiation. The crystallite average size was calculated using the Warren and Scherrer formulae.[27] Instrumental broadening was evaluated on a standard Si sample.

Results

In Fig. 1(A) and 2(A) the TG curves are reported for the A1 and A2 aerogels respectively, while in Fig. 1(B) and 2(B) the corresponding DTA curves are shown.

The A1 aerogel samples show a larger mass loss in the low temperature range than the A2 samples while the total mass loss is larger for the A2 samples compared to the A1 ones. The mass loss at low temperature is due to the removal of residual solvent and/or adsorbed water; the mass loss in the range between 250 and 500 °C, which corresponds to exothermic peaks in the DTA curves, is ascribed to the combustion of ethoxy groups resulting from the esterification of silanols by the ethanol present in the autoclave during high temperature supercritical drying.[28] The mass loss due to the combustion of organics is higher in the A2 samples because of the use of 99% EtOH in the autoclave. Moreover, the combustion of organics occurs over a temperature range which depends on the Fe : Co ratio. In fact, the exothermic peaks are located at a lower temperature for the Fe_{100} samples and they shift towards a higher temperature with increasing cobalt content in both the A1 and A2 samples. For almost all samples the combustion of the organics gives rise to one intense peak plus some peaks with a much lower intensity. In A2-$Fe_{70}Co_{30}$ two peaks of similar intensity are present. The thermal analysis measurements were also carried out on the samples treated at 350 °C indicating that most of the organics are removed by calcination.

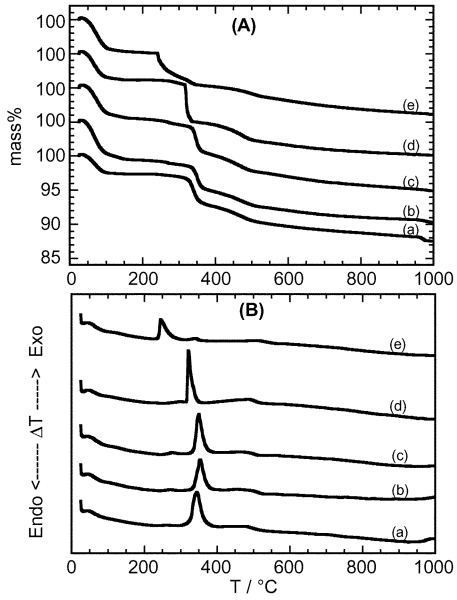

Fig. 1 TG (A) and DTA (B) curves for the A1 aerogels as dried. (a) Co_{100}, (b) $Fe_{30}Co_{70}$, (c) $Fe_{50}Co_{50}$, (d) $Fe_{70}Co_{30}$, (e) Fe_{100}.

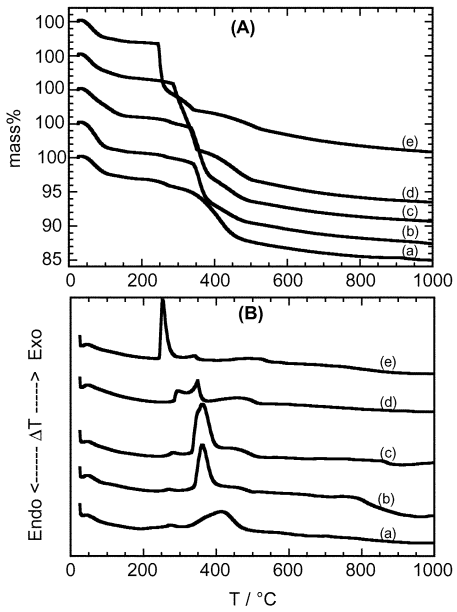

Fig. 2 TG (A) and DTA (B) curves for the A2 aerogels as dried. (a) Co_{100}, (b) $Fe_{30}Co_{70}$, (c) $Fe_{50}Co_{50}$, (d) $Fe_{70}Co_{30}$, (e) Fe_{100}.

In Fig. 3 an example of the typical physisorption isotherms presented by the A1 and A2 samples are shown. The isotherms of the A1 samples can be classified as IV-type,[21,29,30] which is characteristic of a porous structure mainly containing mesopores, featuring an H1 type hysteresis loop.[21,31] The shape of the isotherms observed for the A2 samples indicates a microporous texture, with a high nitrogen uptake at low

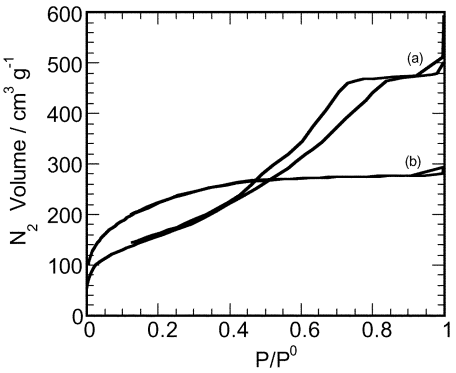

Fig. 3 N_2 physisorption isotherms for the A1-$Fe_{50}Co_{50}$ (a) and A2-$Fe_{50}Co_{50}$ (b) samples.

Table 1 N_2-Physisorption results for the aerogel samples as dried

Sample	S_{TOTAL}/ $m^2\ g^{-1}$	S_t/ $m^2\ g^{-1}$	V_p/ $cm^3\ g^{-1}$	V_{MICRO}/ $cm^3\ g^{-1}$	R_{max}/ Å
A1-Fe_{100}	870	875	1.8873	0.0005	44
A1-$Fe_{70}Co_{30}$	976	980	1.6763	0.0009	30
A1-$Fe_{50}Co_{50}$	582	508	0.9751	0.0378	20
A1-$Fe_{30}Co_{70}$	748	733	1.4820	0.0105	42
A1-Co_{100}	1060	1016	1.7554	0.0184	45
A2-Fe_{100}	904			0.3208	
A2-$Fe_{70}Co_{30}$	830			0.2944	
A2-$Fe_{50}Co_{50}$	796			0.2826	
A2-$Fe_{30}Co_{70}$	823			0.2899	
A2-Co_{100}	730			0.2499	

relative pressure values. However, a partial type IV character is also observed in the A2-Co_{100}, A2-$Fe_{30}Co_{70}$ and A2-$Fe_{50}Co_{50}$ isotherms and a very small hysteresis loop is present. In Table 1 the specific surface area and the pore volumes are reported for the aerogel samples as dried: very large surface areas are observed for both the A1 and A2 aerogels. The t-plot analysis of the isotherms of the A1 samples confirms that the samples are mainly mesoporous, the micropore volume fraction being less than 1% (V_{micro}/V) for all the aerogels except for the A1-$Fe_{50}Co_{50}$ sample which exhibits the largest micropore contribution ($V_{micro}/V = 4\%$). The surface area is not affected by the heat treatment at 350 °C and it is still very high for the final samples after the reduction treatment, being between 450 and 600 $m^2\ g^{-1}$.

The TEM observations indicate that all the A2 samples as dried present nanoparticles with dimensions of a few nanometers homogeneously dispersed in the silica matrix while the A1 samples with high cobalt content also present some larger particles which are not embedded into the silica matrix. The results are very similar for the samples treated at 350 °C. The microdiffraction patterns of the samples as dried and treated at 350 °C indicate the presence of the Co_3O_4 phase. The samples after thermal treatment in hydrogen flow present a homogeneous dispersion of round nanoparticles as seen in Fig. 4, where some examples of TEM bright field micrographs are reported. Crystallite size distribution, which was derived from more than 500 particles in the dark field micrographs, could be well reproduced by a log-normal law[32] with an average diameter, $<D>$, between 8 and 9 nm and standard deviation, σ, between 0.4 and 0.5 in all the samples containing both Fe and Co. Similar values were also obtained for the A1-Fe_{100} and A2-Fe_{100} while $<D>$ is about 5 nm for the

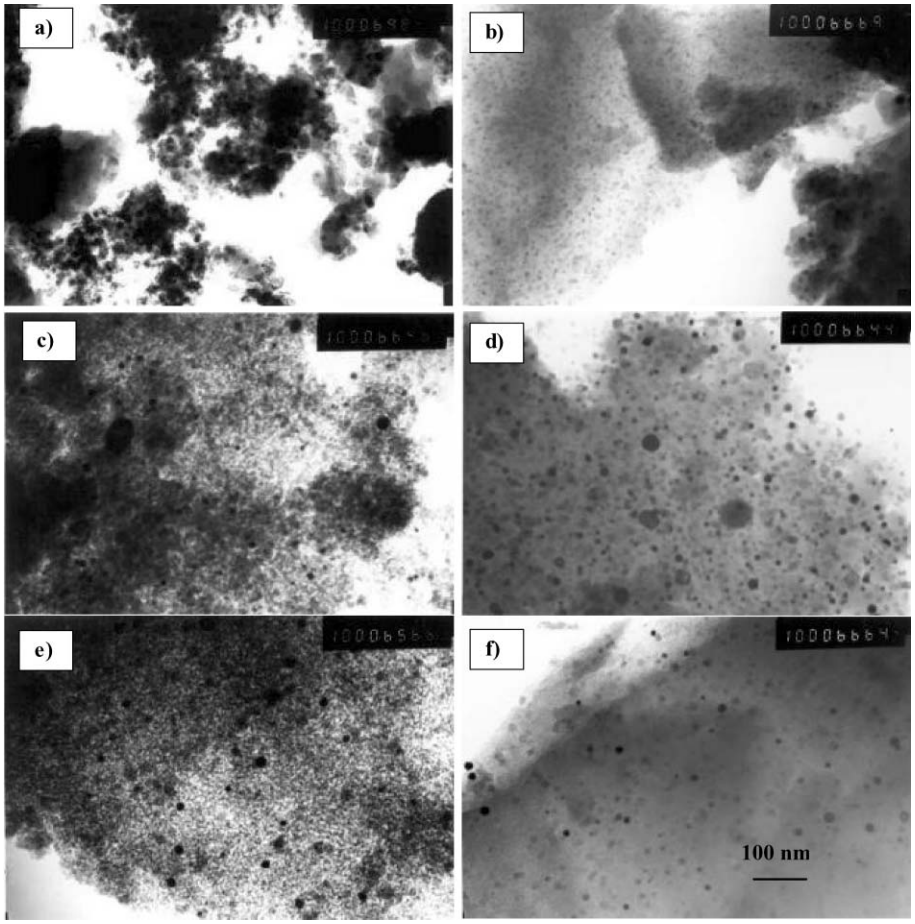

Fig. 4 TEM bright field micrographs of the samples reduced at 800 °C. (a) A1-Co_{100}, (b) A2-Co_{100}, (c) A1-$Fe_{70}Co_{30}$, (d) A2-$Fe_{70}Co_{30}$, (e) A1-Fe_{100}, (f) A2-Fe_{100}.

A1-Co_{100} and 3 nm for the A2-Co_{100}. In the A1-Co_{100} some particles not embedded into silica are also detectable.

The TEM micrographs also show a different porous structure between A1 and A2 samples; in fact pores larger than 2 nm are evident in the A1 samples while the pores are much smaller in the A2 samples.

The XRD spectra for the A1 aerogel samples are reported in Fig. 5(A). All the spectra show a broad halo due to the amorphous silica matrix. In the spectrum of A1-Co_{100} sample peaks due to Co_3O_4 are clearly evident superimposed on the halo;[33] also in the spectra of the samples containing both iron and cobalt the only evident peaks are those due to Co_3O_4 which become weaker with increasing iron content. In the spectrum of the A1-Fe_{100} sample very broad and weak peaks superimposed on the silica halo are barely detectable which might be due to the formation of ferrihydrite,[33] a poorly crystalline ferric oxyhydroxide, as already observed in Fe_2O_3–SiO_2 aerogel nanocomposites.[19]

Similar results were also obtained for the A2 aerogel samples as can be inferred from the XRD spectra, which are reported in Fig. 5(B). The main difference in comparison with the A1 samples is the broadening of the peaks due to the Co_3O_4 phase which is much more pronounced indicating that the average particle size is smaller in the A2 samples compared to the A1 ones. In particular, the average particle size can be estimated to be 3–5 nm in the A2 samples, in agreement with TEM results. The narrower peaks in the A1 samples are in agreement with the presence of some large Co_3O_4 particles not embedded into the amorphous silica, as shown by TEM observations.

The XRD spectra of the A1 and A2 samples after thermal treatment at 350 °C do not show any significant difference with respect to the ones of the aerogel samples as dried.

The spectra after treatment in H_2 flow at 800 °C, which are shown in Fig. 5(C) and 5(D) for the A1 and A2 samples respectively, show that the reduction of the iron and cobalt intermediate phases is complete, since no peak due to oxides is present any more. The spectra of the A1-Fe_{100} and A1-$Fe_{70}Co_{30}$ samples show crystalline peaks which are due to bcc α-Fe and to bcc FeCo alloy respectively.[33] On the other hand, the spectrum of the A1-$Fe_{50}Co_{50}$ sample also shows a weak peak which can be ascribed to fcc Co;[33] the peaks due to the fcc phase are stronger in the spectrum of the A1-$Fe_{30}Co_{70}$ and are the only detectable peaks for the A1-Co_{100} sample. From the spectra of the A2 samples it can be inferred that the bcc phase is the only phase present in the A2-Fe_{100}, A2-$Fe_{70}Co_{30}$ and A2-$Fe_{50}Co_{50}$ samples; a faint peak due to fcc Co is detectable in the spectrum of the A2-$Fe_{30}Co_{70}$ sample together with the peaks of the bcc phase while in the spectrum of A2-Co_{100} only peaks due to fcc Co are visible. The average crystallite size is between 10 and 12 nm apart from the Co_{100} samples where the average size is about 6 nm for the A2-Co_{100} and 70 nm for the A1-Co_{100} sample. The values are in agreement with TEM observations if we take into account the presence of some large particles not embedded into the silica matrix in the A1-Co_{100} sample.

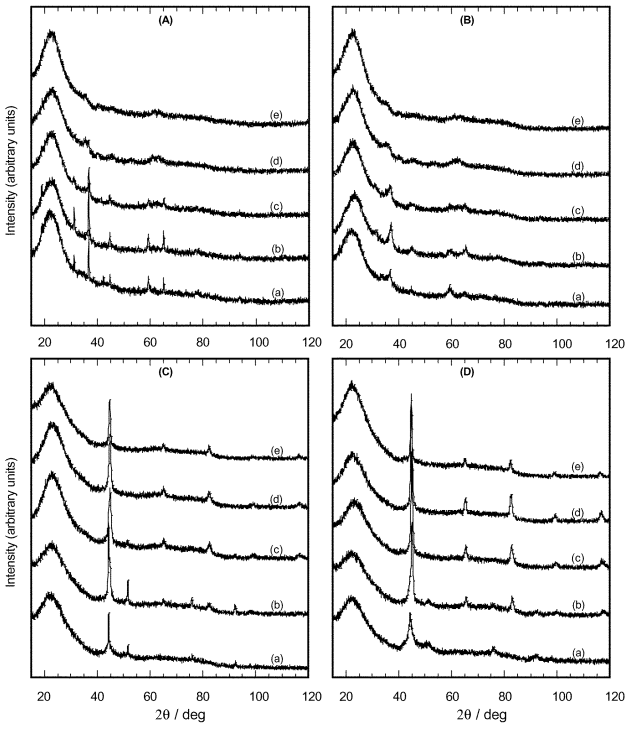

Fig. 5 XRD spectra for the A1 samples as dried (A), A2 samples as dried (B), A1 samples reduced at 800 °C (C), A2 samples reduced at 800 °C (D). (a) Co_{100}, (b) $Fe_{30}Co_{70}$, (c) $Fe_{50}Co_{50}$, (d) $Fe_{70}Co_{30}$, (e) Fe_{100}.

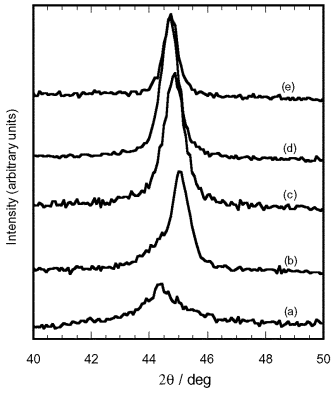

Fig. 6 Detail of the XRD spectra for the A2 samples reduced at 800 °C. (a) Co_{100}, (b) $Fe_{30}Co_{70}$, (c) $Fe_{50}Co_{50}$, (d) $Fe_{70}Co_{30}$, (e) Fe_{100}.

In Fig. 6 the enlargement of the XRD spectra in the region of the most intense peak is presented for the A2-Fe_xCo_{100-x} samples. It can be noticed that the position of the peak in the FeCo–SiO_2 samples shifts towards higher angles as the Co content increases, in accordance with the cell parameters of Fe_xCo_{100-x} bcc alloys which decrease with cobalt content.[33] This indicates that alloy nanoparticles with a composition corresponding to the starting Fe : Co ratio are obtained. A shoulder at low θ is detectable only in the A2-$Fe_{30}Co_{70}$ sample confirming the presence of a small amount of fcc Co in this sample. A similar analysis of the position of the most intense peak in the A1 samples indicates that alloy nanoparticles are formed whose composition is always $Fe_{70}Co_{30}$ and they are accompanied by an increasing amount of fcc Co as the cobalt content increases.

Discussion

This study has shown that FeCo–SiO_2 nanocomposites in the form of aerogels can be prepared by high temperature supercritical drying of alcogels obtained starting from TEOS and nitrate precursors.

The supercritical drying procedure is shown to be able to produce nanocomposites with very large surface areas and pore volumes. As already reported for NiO–SiO_2, Fe_2O_3–SiO_2 systems and for their silica matrix the porous structure can be tuned by correct choice of the experimental conditions for the supercritical drying.[18–20] In particular, N_2-physisorption results indicate that the A1 aerogel samples are mainly mesoporous while the A2 samples have a mainly microporous structure, although minor variations in the texture are also detected as a function of sample composition. The porous structure seems to affect the structural evolution of the samples during the further treatments towards the final nanocomposites.

The decomposition of the metal precursors is practically complete in the autoclave since no evidence of nitrates appears

in the XRD spectra of all the aerogel nanocomposites as dried. This is not surprising since the iron and cobalt nitrates decompose below 330 °C, which is the temperature reached in the autoclave before solvent evacuation, as determined by performing the TG of the starting iron and cobalt nitrate precursors.

The decomposition of cobalt nitrate gives rise to Co_3O_4 nanoparticles whose crystalline peaks are evident in the XRD spectra; on the other hand, iron nitrate decomposes giving rise to a disordered iron oxide hydroxide which is almost undetectable in the XRD spectra. However, the faint peaks can be attributed to the formation of 6-line ferrihydrite as already observed for Fe_2O_3–SiO_2 aerogel nanocomposites;[19] this has been also confirmed by X-ray absorption spectroscopy.[34] The formation of ferrihydrite and Co_3O_4 influences the calcination of the organics which are present in the samples after supercritical drying. In particular, it seems that the crystalline Co_3O_4 nanoparticles make the diffusion of the oxygen more difficult so that the combustion of organics is observed at increasing temperatures as the Co content grows.

No indication of the formation of iron–cobalt mixed oxides was observed either in the samples as dried or after calcination at 350 °C. In particular, the XRD spectra of the nanocomposites after calcination at 350 °C are practically coincident with those of the sample as dried showing that the only effect of the calcination treatment is the combustion of the organics present in the samples after supercritical drying.

The XRD results indicate that the Co_3O_4 mean crystallite size decreases from the A1 to A2 samples as a consequence of their porous structure while TEM observations show that some Co_3O_4 is not embedded into the silica matrix in the A1 samples with a high Co content. The reduction treatment gives rise to the formation of bcc Fe in the A1-Fe_{100} and A2-Fe_{100} samples and to fcc Co in the A1-Co_{100} and A2-Co_{100} samples indicating that ferrihydrite and Co_3O_4 are reduced to the corresponding metals. It should be noted that bcc α-Fe is the phase stable at room temperature while fcc β-Co is generally stable at temperatures higher than 450 °C, the phase stable at room temperature being the hcp α-Co. However, the fcc phase is frequently retained at room temperature particularly when particle size is in the nanometer range.[35,36]

In the samples containing both iron and cobalt the formation of the expected bcc FeCo alloy nanoparticles is obtained; this requires an interdiffusion process between iron and cobalt since they do not form mixed oxides before the reduction treatment. The interdiffusion process is favored by a high surface area and a large contact area between the particles. The different behavior between the A1 and A2 samples cannot be ascribed to different surface area values which are very similar for the two series of samples. On the other hand, the contact area between the Co_3O_4 and the ferrihydrite nanoparticles is much lower in the A1 samples where there are larger Co_3O_4 nanoparticles and some are not embedded into the matrix. As a consequence, the final A2 samples contain FeCo alloy nanoparticles whose composition exactly corresponds to the starting Fe : Co molar ratio while in the A1 samples the interdiffusion is only able to produce an FeCo alloy with a large iron content, the remaining cobalt being present as a separate nanophase. It should be pointed out that a small quantity of oxides and fcc Co could be undetectable in the XRD spectra. However, a careful investigation of the position of the main bcc reflection supports the conclusion that the alloy of the desired composition is obtained in the A2 samples. This has also been confirmed for the A2-$Fe_{50}Co_{50}$ sample by EXAFS spectroscopy[34] since the spectra of the sample at both the Fe and Co K-edges are extremely similar to bcc-Fe. The same EXAFS investigation has also confirmed the simultaneous presence of a bcc alloy together with some fcc Co in the A1-$Fe_{50}Co_{50}$ sample.

It is well known that FeCo alloys near the equiatomic composition are stable at room temperature in an ordered phase (α′-CsCl structure) which transforms into the disordered phase (α-bcc) at higher temperatures.[37] However, it is not possible to distinguish the ordered and disordered phases by XRD since the superlattice lines cannot be observed, the X-ray scattering factors of Fe and Co being too similar.

It should be noted that previous results on xerogel samples of similar compositions showed that the use of the same nitrate precursors does not give rise to the formation of the FeCo alloy even if the samples calcined at 350 °C showed very similar XRD spectra to the A2 samples.[15] It is very likely that the reduction and the interdiffusion process are much easier in the aerogel samples as a consequence of the much larger surface area.

The average particle size of the nanoparticles in the final FeCo–SiO_2 nanocomposites are around 10 nm both in the A1 and the A2 samples. The relatively large values of the particle size also in the A2 samples are probably due to the high temperature of the reduction treatment which favors the interdiffusion and therefore the growth of the particles. In fact, the A2-Co_{100} sample presents much smaller nanoparticles with an average size of a few nanometers. The average particle size of the FeCo alloy nanoparticles is very similar to those found in the FeCo–SiO_2 xerogel nanocomposites obtained starting from acetate precursors,[15] showing that in the case of aerogels the nitrate precursors can give the same satisfactory results with the advantage of obtaining samples with high surface area and pore volume.

Preliminary results indicate that the reduction treatment can be carried out in the A2 aerogel samples at a lower temperature so that FeCo nanoparticles with a smaller particle size can be obtained.

The magnetic characterization of the samples, which will be the subject of a further paper, indicates that the nanoparticles behave as superparamagnets which are still blocked at room temperature and their hysteresis loops exhibit coercive fields up to 900 Oe.

Conclusions

FeCo–SiO_2 nanocomposite aerogels were obtained by the sol–gel method; samples with different textural characteristics were obtained by varying the experimental conditions of the supercritical drying process. In particular, two different series of aerogels were obtained which are mainly mesoporous or microporous respectively.

The porous structure has a strong influence on the formation of FeCo alloy nanoparticles in the silica matrix. XRD and TEM show that Co_3O_4 and ferrihydrite nanoparticles are present both in the samples as dried and calcined at 350 °C; Co_3O_4 nanoparticles are smaller in the microporous samples than in the mesoporous ones. In the reduction treatment Co_3O_4 is converted to fcc Co while ferrihydrite is converted to bcc Fe and the interdiffusion between the two metals leads to the formation of FeCo alloy nanoparticles. When the size of the original Co_3O_4 nanoparticles is small as in the microporous aerogels the interdiffusion process can proceed until all the precursors are completely transformed into the alloy of the desired composition while the interdiffusion is not complete in the mesoporous samples due to the larger size of the Co_3O_4 nanoparticles.

Acknowledgement

The authors wish to thank MURST for financial support.

References

1 G. Piccaluga, A. Corrias, G. Ennas and A. Musinu, *Sol-Gel Preparation and Characterization of Metal-Silica and Metal*

Oxide-Silica Nanocomposites, Material Research Foundation, Vol. 13, Trans Tech Publications Ltd., Uetikon, Switzerland, 2000.
2 S. Roy, D. Das, D. Chakravorty and D. C. Agrawal, *J. Appl. Phys.*, 1993, **74**, 4746.
3 S. Roy and D. Chakravorty, *J. Phys.: Condens. Matter*, 1994, **6**, 8599.
4 J. P. Carpenter, C. M. Lukehart, S. B. Milne, D. O. Henderson, R. Mu and S. R. Stock, *Chem. Mater.*, 1997, **9**, 3164.
5 G. T. De, *J. Sol-Gel Sci Technol.*, 1998, **11**, 289.
6 A. Basumallick, G. C. Das and S. Mukherjee, *Thermochim. Acta*, 1999, **325**, 167.
7 G. Ennas, A. Falqui, G. Piccaluga, S. Solinas, D. Gatteschi, C. Sangregorio and A. Benedetti, *Z. Naturforsch. A: Phys. Sci.*, 2000, **55**, 581.
8 C. Cannas, D. Gatteschi, A. Musinu, G. Piccaluga and C. Sangregorio, *J. Phys. Chem. B*, 1998, **102**, 7721.
9 C. Cannas, M. Casu, A. Lai, A. Musinu and G. Piccaluga, *J. Mater. Chem.*, 1999, **9**, 1765.
10 D. Das, M. Pal, E. D. Bartolomeo, E. Traversa and D. Chakravorty, *J. Appl. Phys.*, 2000, **88**, 6856.
11 F. Del Monte, M. P. Morales, D. Levy, A. Fernandez, M. Ocana, A. Roig, E. Molins, K. O'Grady and C. J. Serna, *Langmuir*, 1997, **13**, 3627.
12 D. I. Bardos, *J. Appl. Phys.*, 1969, **40**, 1371.
13 M. S. Lataifeh, *J. Phys. Soc. Jpn.*, 2000, **69**, 248.
14 X. G. Li, T. Murai, T. Saito and S. Takahashi, *J. Magn. Magn. Mater.*, 1988, **190**, 277.
15 G. Ennas, M. F. Casula, A. Falqui, D. Gatteschi, G. Marongiu, G. Piccaluga, C. Sangregorio and G. Pinna, *J. Non-Cryst. Solids*, 2001, **293–295**, 1.
16 C. J. Brinker and G. W. Scherer, *Sol-gel Science*, Academic Press, San Diego, 1990.
17 G. M. Pajonk, *Catal. Today*, 1997, **35**, 319.
18 M. F. Casula, A. Corrias and G. Paschina, *J. Mater. Res.*, 2000, **15**, 2187.
19 M. F. Casula, A. Corrias and G. Paschina, *J. Non-Cryst. Solids*, 2001, **293–295**, 25.
20 M. F. Casula, M. Casu, A. Corrias and G. Paschina, *J. Non-Cryst. Solids*, submitted.
21 F. Rouquerol, J. Rouquerol and K. S. W. Sing, *Adsorption by Powders and Porous Solids: Principles, Methodology and Applications*, Academic Press, London, 1999.
22 S. Brunauer, P. H. Emmet and E. Teller, *J. Am. Chem. Soc.*, 1938, **60**, 309.
23 S. Storck, H. Bretinger and W. F. Maier, *Appl. Catal. A*, 1998, **174**, 137.
24 B. C. Lippens and J. H. De Boer, *J. Catal.*, 1965, **4**, 319.
25 A. Lecloux and J. P. Pirard, *J. Colloid Interface Sci.*, 1979, **70**, 265.
26 M. M. Dubinin, *Q. Rev. Chem. Soc.*, 1955, **9**, 101.
27 H. P. Klug and L. E. Alexander, *X-ray Diffraction Procedures*, Wiley, New York, 1974.
28 M. Prassas, J. Phalippou and J. Zarzycki, *J. Mater. Sci.*, 1984, **19**, 1656.
29 K. S. W. Sing, D. H. Everett, R. A. W. Haul, L. Moscou, R. A. Pierotti, J. Rouquerol and T. Siemieniewska, *Pure Appl. Chem.*, 1985, **57**, 603.
30 J. Rouquerol, D. Avnir, C. W. Fairbridge, D. H. Everett, J. H. Haynes, N. Pernicone, J. D. F. Ramsay, K. S. W. Sing and K. K. Unger, *Pure Appl. Chem.*, 1994, **66**, 1667.
31 S. Brunauer, L. S. Deming, W. S. Deming and E. Teller, *J. Am. Chem. Soc.*, 1940, **62**, 1723.
32 R. Kaiser and G. Miskolczy, *J. Appl. Phys.*, 1970, **41**, 1064.
33 PDF-2 File, JCPDS International Centre for Diffraction Data, 1601 Park Lane, Swarthmore, USA.
34 M. F. Casula, A. Corrias and G. Navarra, *J. Sol-Gel Sci. Technol.*, in press.
35 A. Corrias, G. Ennas, G. Marongiu, A. Musinu and G. Paschina, *J. Mater. Res.*, 1993, **8**, 1327.
36 O. Kitakami, H. Sato, Y. Shimada, F. Sato and M. Tanaka, *Phys. Rev. B: Conden. Matter*, 1997, **56**, 13849.
37 J. H. J Scott, K. Chowdary, Z. Turgut, S. A. Majetich and M. E. McHenry, *J. Appl. Phys.*, 1999, **85**, 4409.